THE GEOLOGICAL SOCIETY OF AMERICA®

Fault-controlled dolomitization in a rift basin

Cathy Hollis[1], Eivind Bastesen[2], Adrian Boyce[3], Hilary Corlett[1]*, Robert Gawthorpe[2], Jesal Hirani[1†], Atle Rotevatn[2], and Fiona Whitaker[4]

[1]School of Earth and Environmental Science, University of Manchester, Manchester M13 9PL, UK
[2]Department of Earth Science, University of Bergen, Bergen N-5020, Norway
[3]Scottish Universities Environmental Research Centre, East Kilbride G75 0QF, UK
[4]School of Earth Sciences, University of Bristol, Bristol BS8 1RJ, UK

ABSTRACT

There are numerous examples of fault-controlled, so-called hydrothermal dolomite (HTD), many of which host economic mineral deposits or hydrocarbons, but there remains a lack of consensus as to how they form. In particular, multiple phases of diagenetic overprinting can obscure geochemical fingerprints. Study of a Cenozoic succession with a relatively simple burial history here provides new insights into the development of differentially dolomitized beds. The Hammam Faraun fault (HFF) block within the Suez Rift, Egypt, hosts both massive and stratabound dolostone bodies. Non-fabric-selective massive dolostone is limited to the damage zone of the fault, while fabric-selective stratabound dolostone bodies penetrate nearly 2 km into the footwall. Oligo-Miocene seawater is interpreted to have been drawn down discrete faults into a deep aquifer and convected upwards along the HFF. Escape of fluids from the incipient HFF into the lower Thebes Formation led to differential, stratabound dolomitization. Once the HFF breached the surface, fluid circulation focused along the fault plane to form younger, massive dolostone bodies. This study provides a snapshot of dolomitization during the earliest phases of extension, unobscured by subsequent recrystallization and geochemical modification. Contrary to many models, stratabound dolomitization preceded non-stratabound dolomitization. Fluids were hydrothermal, but with little evidence for rapid cooling and brecciation common to many HTD bodies. These results suggest that many of the features used to interpret and predict the geometry of HTD in the subsurface form during later phases of structural deformation, perhaps overprinting less structurally complex dolomite bodies.

INTRODUCTION AND GEOLOGICAL SETTING

Hydrothermal dolomite (HTD) forms when dolomitization occurs from fluids that are significantly hotter than the ambient rock (Machel and Lonnee, 2002). HTD has become common parlance for dolomite formed proximal to faults, with a non-stratabound core and stratabound margin, commonly localized around normal and strike-slip faults, with little consensus on the source of fluid or Mg^{2+} or the process for dolomitization (Davies and Smith, 2006). Furthermore, most case studies are in pre-Cenozoic strata, so multiple phases of structural reactivation, fluid flow, and recrystallization are likely to have obscured the geochemical fingerprint of the oldest dolomite phases. In contrast, the simple burial and exhumation history of the dolostone bodies in this study allows insight into fluid flux and dolomitization during early rifting.

The Suez Rift in Egypt (Fig. 1) is the aborted arm of the Red Sea rift. The Hammam Faraun fault (HFF) defines the western side of the HFF block and tips out northward (Fig. 1). The partially dolomitized Eocene (Ypresian) Thebes Formation (Fig. 1B) is exposed in the footwall, overlying the Paleocene Esna Shale, carbonate-dominated Cretaceous strata, and the Paleozoic Nubian Sandstone, composed largely of quartz arenite (Nabawy et al., 2009). The overlying syn-rift succession is dominantly siliciclastic, overlain by Miocene evaporites (Moustafa, 2003). Rifting was initiated in the Oligocene (26 Ma) along numerous small faults until displacement localized on the HFF by ca. 17 Ma (rift climax; Gawthorpe et al., 2003). This resulted in offset of nearly 5 km and formed an ~500-m-wide damage zone that is bounded by discontinuous fracture corridors (Fig. 1C; Rotevatn and Bastesen, 2014).

ANALYTICAL METHODS

All samples were georeferenced in the field and prepared as polished thin sections, and matching offcuts were microdrilled for isotopic analysis or powdered for bulk X-ray diffraction and rare earth element (REE) analysis. Full analytical details are provided by Hirani (2014). See the GSA Data Repository[1] for dolostone body and limestone data.

DOLOMITIZATION ON THE HAMMAM FARAUN FAULT BLOCK

The Thebes Formation comprises debrites and foraminiferal grainstone turbidites embedded in skeletal wacke- to packstone, interpreted as platform slope deposits (Hirani, 2014). Two types of dolostone bodies occur: massive and stratabound (Figs. 1 and 2A).

Two massive dolostone bodies, each ~80 m thick and up to 500 m wide, are non–facies selective, fabric destructive, dark brown to red, pervasively fractured, and chaotically brecciated (Fig. 2B). The bodies have a sharp basal contact with the underlying Esna Shale. Laterally they terminate as short (<100-m-long) tongues or abruptly against NNE-SSW– and NW-SE–trending fracture corridors (Fig. 1C). Dolomite is non-ferroan with nonplanar textures (*sensu* Sibley and Gregg, 1987) and a mottled bright red and orange cathodoluminescence (CL), commonly with cloudy cores and a clear cement rim (Figs. 2C and 2D). Bulk-rock stable $\delta^{13}C_{dolomite}$ values have a narrow range but $\delta^{18}O_{dolomite}$ values are scattered (Fig. 3A). REE profiles have negative Ce and positive La anomalies and a flattened heavy REE (HREE) profile (Fig. 3B). $^{87}Sr/^{86}Sr$ values are bimodal and range from 0.70811 to 0.70858 (Fig. 3C).

Stratabound dolostone bodies are more numerous, 5–300 m long and 25 cm to 15 m thick, weakly fabric preserving, and dark brown in color. They formed exclusively within debrite and grainstone turbidite beds with sharp upper and basal contacts and abrupt lateral terminations (Fig. 2E). The bodies extend discontinuously into

*Current address: Alberta Geological Survey, Edmonton, Alberta T6B 2X3, Canada.
†Current address: Badley Ashton and Associates Ltd., Horncastle LN9 6PB, UK.

[1]GSA Data Repository item 2017057, data for dolostone bodies and limestone (carbon and oxygen stable isotope, $^{87}Sr/^{86}Sr$, rare earth element, major element bulk rock, and bulk rock XRD), and formation thicknesses and permeability for pre- and syn-rift sediments on the Hammam Faraun fault block, is available online at www.geosociety.org/datarepository/2017 or on request from editing@geosociety.org.

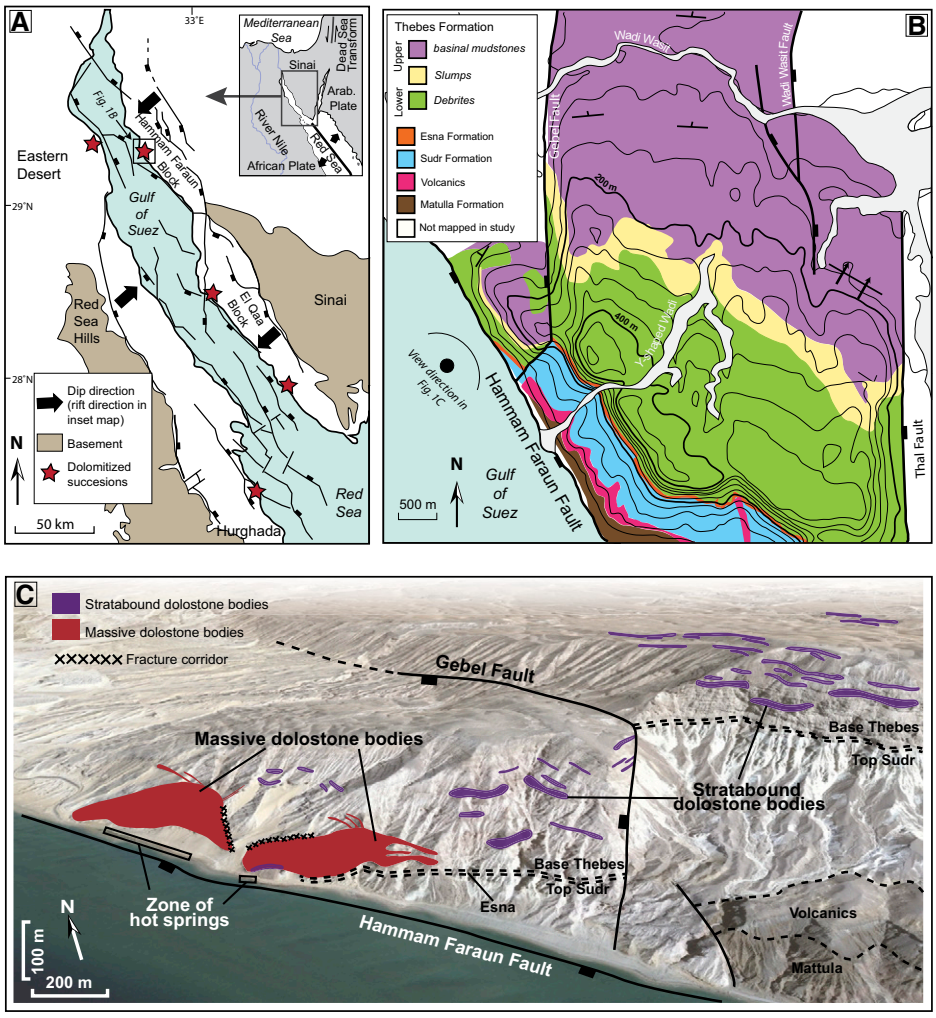

Figure 1. A: Regional geological map and location map (inset), Suez Rift, Egypt. B: Geological map of Hammam Faraun fault (HFF) block (modified after Moustafa, 2003). C: HFF block viewed looking northeast (see B).

the footwall for up to 2 km, decreasing in frequency away from the HFF, and are offset by the Gebel fault (Fig. 1C). Dolomite is non-ferroan with planar-*s* and nonplanar cloudy core–clear rimmed fabrics (*sensu* Sibley and Gregg, 1987; Fig. 2F). Under CL, the cores luminesce bright red and orange while clear rims have a concentrically zoned, yellow-green-orange luminescence (Fig. 2G). Bulk stable isotope values are depleted relative to the unaltered limestone, with a narrow range (Fig. 3A). REE profiles have negative Ce and positive La anomalies and depleted and flattened HREE profile (Fig. 3B). $^{87}Sr/^{86}Sr$ ranges from 0.70806 to 0.70824 (Fig. 3C).

Timing, Fluid Composition, and Temperature

The stratabound dolostone bodies are offset by the Gebel fault, which became inactive in the early Miocene (Gawthorpe et al., 2003), suggesting that they formed prior to the rift climax. Because the massive dolostone bodies are densely fractured and brecciated, and partially bounded by fracture corridors, they are interpreted to be located within the damage zone of the HFF. Hence the massive dolostone must have formed at the rift climax, after localization of deformation on the HFF. $^{87}Sr/^{86}Sr$ ratios for the stratabound dolostone appear to correspond to late Oligocene seawater (ca. 28–24 Ma), coincident with rift initiation. $^{87}Sr/^{86}Sr$ ratios for the massive dolostone are bimodal: a subset of samples has ratios that match Oligocene seawater (ca. 26–24 Ma), but the majority have an apparently younger age that is consistent with the rift climax (ca. 22–17 Ma; Fig. 3C).

The negative Ce and positive La anomalies and slightly flattened HREE profiles of both types of dolostone bodies compared to the host limestone imply that they record the REE signature of suboxic seawater (Haley et al., 2004). The $\delta^{13}C$ for all dolostone bodies is more depleted than for the precursor limestone (Fig. 3A) and Oligocene-Miocene seawater (2‰–4‰; Veizer and Prokoph, 2015) and may reflect an input of isotopically light carbon by degradation of organic matter. Both observations imply dolomitization at fluid-rock ratios that were high enough to overprint the geochemical signature of the precursor limestone (Banner et al., 1988).

Using the method of Matthews and Katz (1977), the lightest and heaviest $\delta^{18}O_{dolomite}$ for each body, and $\delta^{18}O_{seawater} = -1‰$ to +0‰ SMOW (standard mean ocean water) (Veizer and Prokoph, 2015), the stratabound dolostone is calculated to have formed at ~40–70 °C and the massive dolostone at ~40–100 °C. Assuming a geothermal gradient of 45 °C km^{-1} and surface seawater temperatures of 25 °C, ambient rock temperatures would have been ~56 °C at maximum burial (Hirani, 2014), so dolomitizing fluids can mostly be interpreted as hydrothermal. No primary fluid inclusions suitable for thermometry were identified, but the calculated temperatures are consistent with those measured by clumped isotope analysis (51–75 °C, $n = 5$; Hirani, 2014). If fluid-rock interaction enriched $\delta^{18}O_{water}$, or seawater became enriched by evaporation, then the temperature of dolomitization could be somewhat higher than estimated (by between 10 and 20 °C, assuming $\delta^{18}O_{water} = +2‰$ SMOW).

Mechanism for Fluid Flux and Dolomitization

Since deposition, the Thebes Formation in the footwall of the HFF has been uplifted and rotated from >550 m burial depth (Hirani, 2014). The only available fluid, within the observed temperature range, of sufficient volume and Mg/Ca ratio for dolomitization, during this period, was seawater. This is consistent with the $^{87}Sr/^{86}Sr$ and REE signature of the dolostones. At rift initiation, the proto–HFF block was dissected by numerous discrete faults. Offset on the incipient HFF was minor, with the fault tip most likely in the Thebes Formation (Gawthorpe et al., 2003). Seawater could have been drawn down the discrete, surface-breaching faults (Fig. 4A) and fluxed into the Nubian Sandstone, the principal aquifer in the region today with permeabilities of several darcys (Nabawy et al., 2009). There, seawater could have been entrained into free convection cells, enhanced by a high heat flux due to rifting (e.g., Garven et al., 1999). The close fit of the $^{87}Sr/^{86}Sr$ ratios to the Oligo-Miocene seawater curve (Fig. 3C) suggests little Sr enrichment of the seawater by fluid-rock interaction during convection, consistent with the inert, quartz-rich composition of the Nubian Sandstone (Nabawy et al., 2009). On reaching the HFF, buoyant, hot fluids could have escaped upwards to discharge laterally into the lower Thebes Formation at the fault tip.

As strain localized onto the HFF, movement on the smaller, discrete faults ceased (Gawthorpe et al., 2003) and uplift of the HFF footwall led to emergence of the footwall, terminating the influx of seawater. Convection could have persisted by drawdown of seawater along faults in the hanging wall of the HFF, as well as by convection directly along the plane of the HFF, which

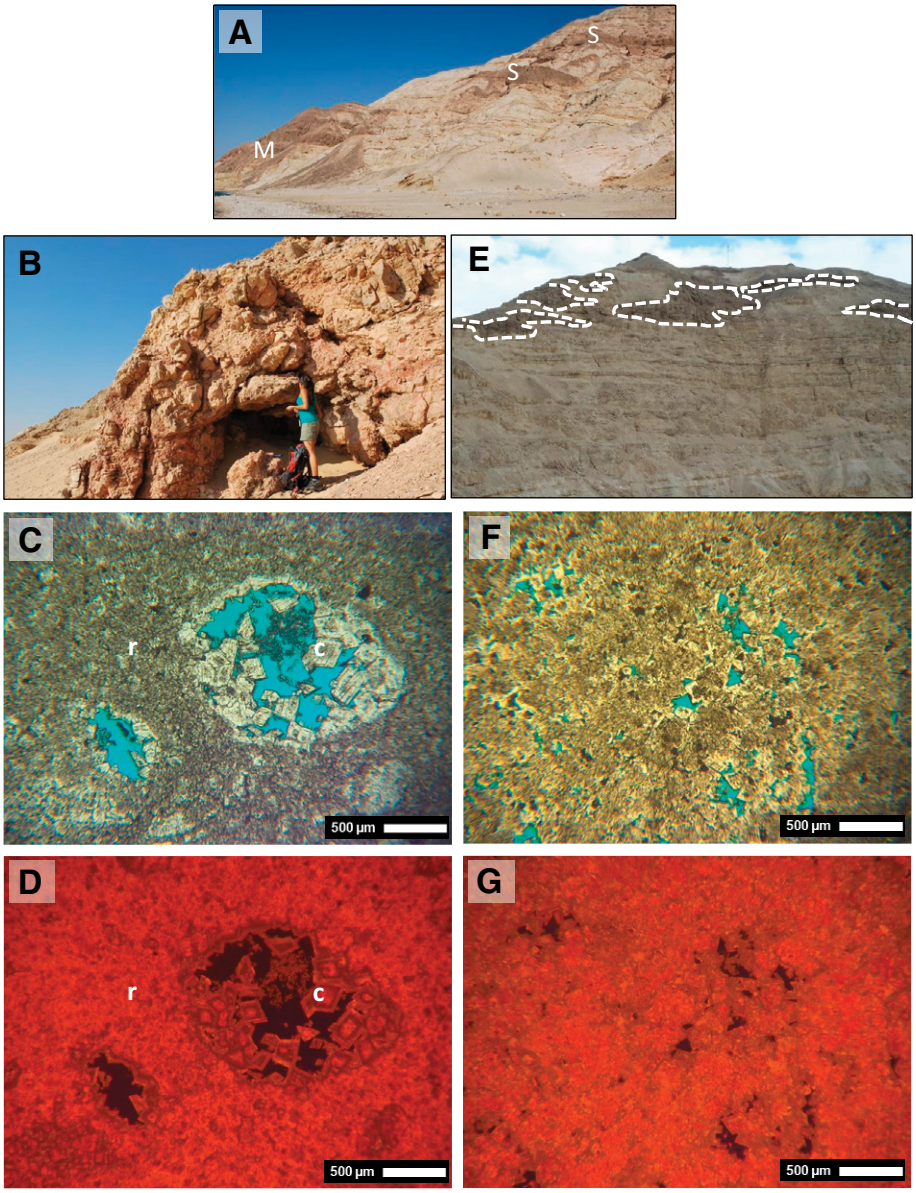

Figure 2. A: Massive dolostone (M) and stratabound dolostone (S) bodies viewed from beach, adjacent to Hammam Faraun fault (HFF), Egypt. B: Chaotic breccia within massive dolostone. C: Massive dolostone in transmitted light showing non-planar replacive dolomite (r) and dolomite cement (c). D: Image C in cathodoluminescence (CL), showing mottled orange-red luminescence. E: Stratabound dolostone (dashed). F: Cloudy core–clear rimmed dolomite within stratabound dolostone (transmitted light). G: CL image of F showing zoned orange-red luminescence.

would have breached the seafloor at this time (Fig. 4B). The restriction of the dolostone bodies to the narrow, highly fractured damage zone suggests limited lateral flux of seawater into the footwall. Given the limited opportunity for fluid mixing, wide-ranging oxygen and $^{87}Sr/^{86}Sr$ ratios in the massive dolostone may reflect multiple phases of dolomitization by numerous passes of seawater at a range of temperatures. As such, the oldest (Oligocene) ages may represent the earliest phases of massive dolomitization or remnant, precursor stratabound dolostone. Formation of the younger (ca. 17 Ma) dolostone could have also been facilitated by the flux of seawater with enhanced solute concentrations as the basin became increasingly isolated, evidenced by the late syn-rift evaporite succession.

IMPLICATIONS AND CONCLUSIONS

Many conceptual models of HTD use a geometrical association of massive and stratabound dolostone to interpret contemporaneous formation by fluid supplied from a fault. This study identifies stratabound dolostone that predates massive dolostone, apparently by several million years, indicating that it is not necessarily valid to assume a syngenetic relationship between massive and stratabound bodies. Instead, although the two types of dolostone bodies may be linked to structural evolution, they can be decoupled in time. At rift initiation, fluid flux appears to have been controlled largely by geothermal convection, resulting in fabric-retentive dolomite in discrete beds with a well-constrained geochemistry. At rift climax, we suggest that intense structural deformation resulted in repeated, transient pulses of fluid within the damage zone of the fault. This led to multiple phases of dolomitization, forming brecciated, non-fabric-retentive, non-stratabound dolostone bodies. Strikingly, several characteristic textural features of HTD, such as saddle dolomite, zebra dolomite, and hydrobreccia (Davies and Smith, 2006), are conspicuously absent on the HFF block. Because the study area has undergone a short and simple history of burial and exhumation, it is possible that such apparently diagnostic HTD textures only

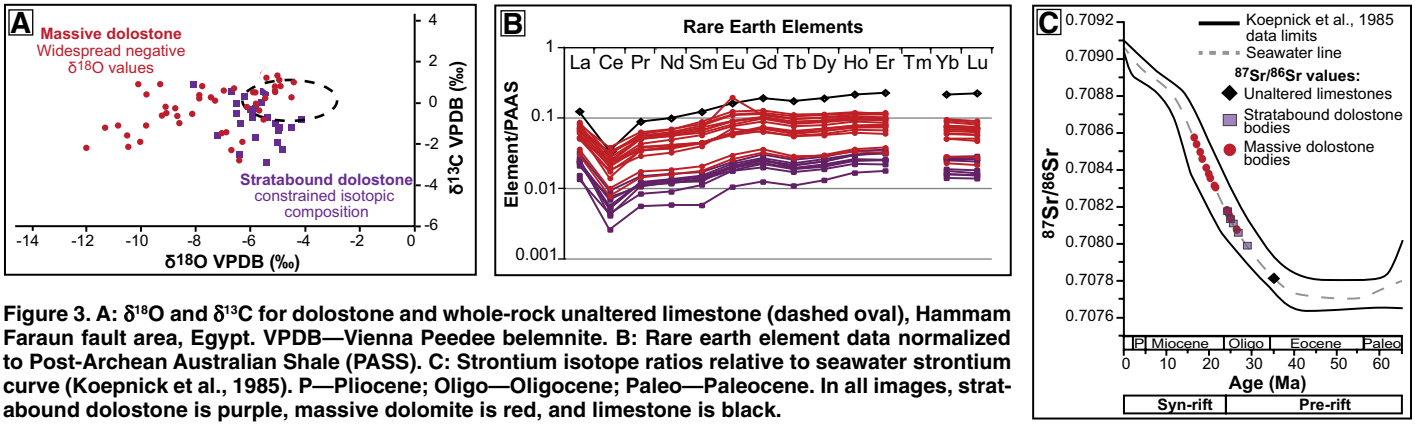

Figure 3. A: $\delta^{18}O$ and $\delta^{13}C$ for dolostone and whole-rock unaltered limestone (dashed oval), Hammam Faraun fault area, Egypt. VPDB—Vienna Peedee belemnite. B: Rare earth element data normalized to Post-Archean Australian Shale (PASS). C: Strontium isotope ratios relative to seawater strontium curve (Koepnick et al., 1985). P—Pliocene; Oligo—Oligocene; Paleo—Paleocene. In all images, stratabound dolostone is purple, massive dolomite is red, and limestone is black.

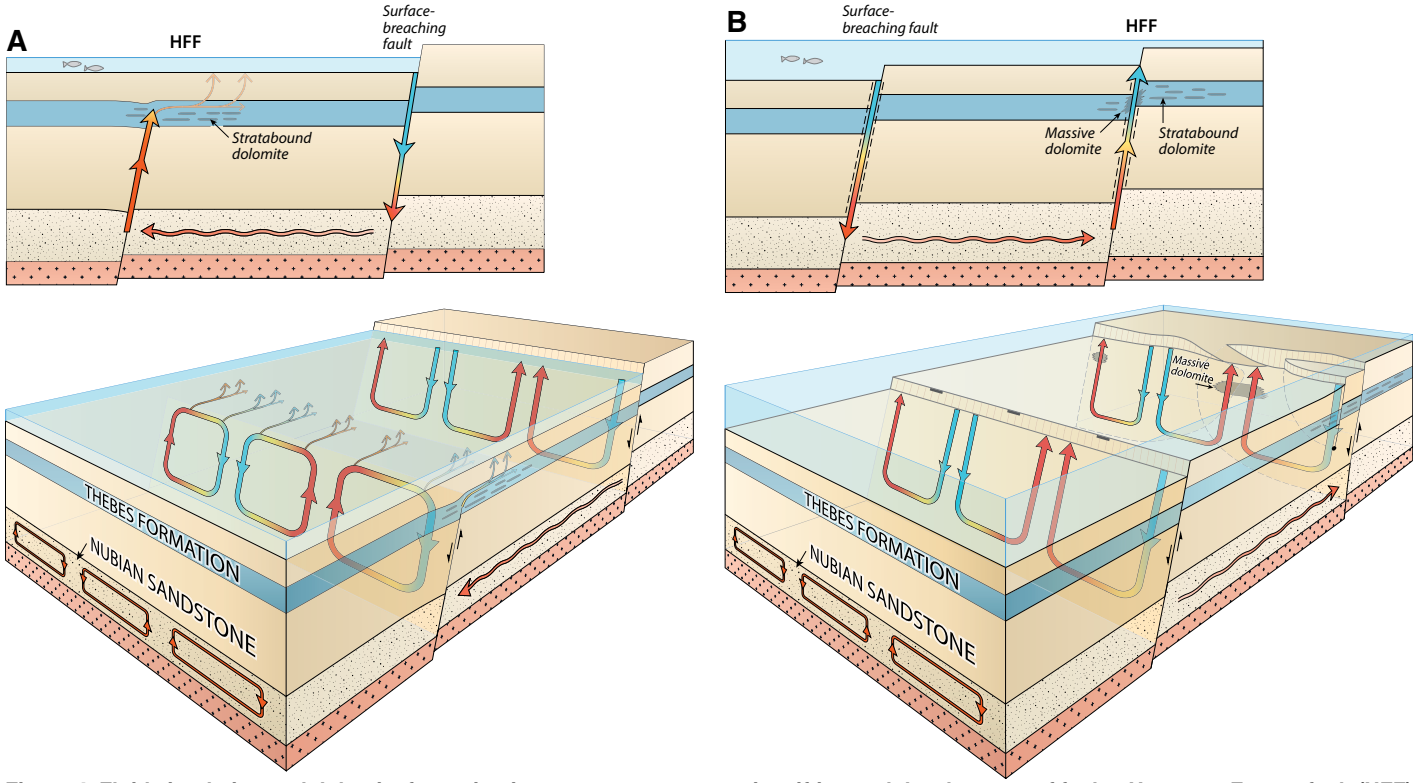

Figure 4. Fluid circulation and dolomite formation in response to progressive rifting and development of faults, Hammam Faraun fault (HFF) area, Egypt. A: Rift initiation. Cool seawater is drawn down discrete open faults on proto-footwall, heated, and convected within Nubian Sandstone. Buoyant, hot fluids circulate up proto-HFF into lower Thebes Formation and react to form stratabound dolostone. B: Rift climax. Deformation is transferred to HFF, which breaches surface. Cold seawater is drawn into convection cells along fault plane, with hot, rising fluids forming massive dolostone in damage zone. Some entrained seawater in Nubian Sandstone may also contribute to circulation.

form during fault reactivation under transpression, when fluid pressures are higher and cooling is more rapid.

ACKNOWLEDGMENTS

This project was funded via Industry Technology Facilitator project 3310PSD by BG-Group, Saudi Aramco, Statoil, and Total. Stable isotope analysis was conducted through Natural Environment Research Council (NERC) Facility award IP-1357-1112 at the NERC Isotope Community Support Facility at SUERC, which also funds Boyce. Thanks to Stefan LaLonde and Germain Bayon, University of Brest, for strontium isotope analysis, and Veerle Vendeginste and Cedric John, Imperial College, London, for clumped isotope analysis. Thanks to Eva Bjorseth who drafted the figures. We also thank editor Bob Holdsworth, and Hans Machel, Jay Gregg, Paul Gillespie, and an anonymous reviewer, whose comments greatly improved the quality of the manuscript.

REFERENCES CITED

Banner, J.L., Hanson, G.N., and Meyers, W.J., 1988, Rare earth element and Nd isotopic variations in regionally extensive dolomites from the Burlington-Keokuk Formation (Mississippian): Implications for REE mobility during carbonate diagenesis: Journal of Sedimentary Petrology, v. 58, p. 415–432, doi:10.1306/212F8DAA-2B24-11D7-8648000102C1865D.

Davies, G., and Smith, L., 2006, Structurally controlled hydrothermal dolomite reservoir facies: An overview: American Association of Petroleum Geologists Bulletin, v. 90, p. 1641–1690, doi:10.1306/05220605164.

Garven, G., Appold, M., Toptygina, V., and Hazlett, T., 1999, Hydrogeologic modelling of the genesis of carbonate-hosted lead-zinc ores: Hydrogeology Journal, v. 7, p. 108–126, doi:10.1007/s100400050183.

Gawthorpe, R.L., Jackson, C.A.L., Young, M.J., Sharp, I.R., Moustafa, A.R., and Leppard, C.W., 2003, Normal fault growth, displacement localisation and the evolution of normal fault populations: The Hammam Faraun fault block, Suez rift, Egypt: Journal of Structural Geology, v. 25, p. 883–895, doi:10.1016/S0191-8141(02)00088-3.

Haley, B., Klinkhammer, G., and McManus, J., 2004, Rare earth elements in pore waters of marine sediments: Geochimica et Cosmochimica Acta, v. 68, p. 1265–1279, doi:10.1016/j.gca.2003.09.012.

Hirani, J., 2014, Diagenetic evaluation of fault/fracture related dolomitisation, Cretaceous-Eocene, Hammam Faraun Fault Block, Gulf of Suez [Ph.D. thesis]: Manchester, UK, University of Manchester, 295 p.

Koepnick, R., Burke, W., Denison, R., Hetherington, E., Nelson, H., Otto, J., and Waite, L., 1985, Construction of the seawater $^{87}Sr/^{86}Sr$ curve for the Cenozoic and Cretaceous: Supporting data: Chemical Geology, v. 58, p. 55–81, doi:10.1016/0168-9622(85)90027-2.

Machel, H., and Lonnee, J., 2002, Hydrothermal dolomite: A product of poor definition and imagination: Sedimentary Geology, v. 152, p. 163–171, doi:10.1016/S0037-0738(02)00259-2.

Matthews, A., and Katz, A., 1977, Oxygen isotope fractionation during the dolomitization of calcium carbonate: Geochimica et Cosmochimica Acta, v. 41, p. 1431–1438, doi:10.1016/0016-7037(77)90249-6.

Moustafa, A.R., 2003, Explanatory notes for the geologic maps of the eastern side of the Suez Rift (western Sinai Peninsula): American Association of Petroleum Geologists Datapages GIS Series 34, 34 p.

Nabawy, B., Geraud, Y., Rochette, P., and Bur, N., 2009, Pore-throat characterization in highly porous and permeable sandstones: American Association of Petroleum Geologists Bulletin, v. 93, p. 719–739, doi:10.1306/03160908131.

Rotevatn, A., and Bastesen, E., 2014, Fault linkage and damage zone architecture in tight carbonate rocks in the Suez Rift (Egypt): Implications for permeability structure along segmented normal faults, *in* Spence, G.H., et al., eds., Advances in the Study of Fractured Reservoirs: Geological Society of London Special Publication 374, p. 79–95, doi:10.1144/SP374.12.

Sibley, D.F., and Gregg, J.M., 1987, Classification of dolomite rock textures: Journal of Sedimentary Research, v. 57, p. 967–975, doi:10.1306/212F8CBA-2B24-11D7-8648000102C1865D.

Veizer, J., and Prokoph, A., 2015, Temperatures and oxygen isotopic composition of Phanerozoic oceans: Earth-Science Reviews, v. 146, p. 92–104, doi:10.1016/j.earscirev.2015.03.008.

Manuscript received 22 July 2016
Revised manuscript received 14 November 2016
Manuscript accepted 16 November 2016

Printed in USA